

Tilings of a bounded region of the plane by maximal one-dimensional tiles

Eduardo J. Aguilar,¹ Valmir C. Barbosa,² Raul Donangelo,^{3, 4} Welles A. M. Morgado,^{5, 6} and Sergio R. Souza^{3, 7, *}

¹*Instituto de Ciéncia e Tecnologia, Universidade Federal de Alfenas, Poços de Caldas, MG 37715-400, Brazil*

²*Programa de Pós-Graduaçao em Ciéncias Computacionais, IME,*

Universidade do Estado do Rio de Janeiro, Rio de Janeiro, RJ 20550-900, Brazil

³*Instituto de Física, Universidade Federal do Rio de Janeiro, Rio de Janeiro, RJ 21941-909, Brazil*

⁴*Instituto de Física, Facultad de Ingeniería, Universidad de la Repùblica, Montevideo 11.300, Uruguay*

⁵*Departamento de Física, Pontifícia Universidade Católica, Rio de Janeiro, RJ 22452-970, Brazil*

⁶*National Institute of Science and Technology—Complex Systems, Teresina, PI 64049-550, Brazil*

⁷*Departamento de Física, ICEX, Universidade Federal Fluminense, Volta Redonda, RJ 27213-145, Brazil*

(Dated: November 25, 2025)

We study the tiling of a two-dimensional region of the plane by K -cell one-dimensional tiles, or K -mers. Unlike previous studies, which typically allowed for one single value of K or sometimes a small assortment of fixed values, here a tiling may concomitantly employ K -mers comprising any number K of cells, provided a maximality constraint is satisfied. In essence, this constraint requires each of the K -mers in use to be as lengthy as possible, given its surroundings in the resulting tiling. Maximality aims to limit the variety of possible tilings while allowing for interesting behavior in terms of the statistical physical observables of interest. In fact, by introducing an energy function based on cell contacts and parameterizing it appropriately, we have been able to observe relatively unexpected behavior, including the suggestion of phase transitions as the system's temperature evolves.

I. INTRODUCTION

Given a finite collection C of tile types, a tiling of the plane is a covering that employs tiles from C only and allows for no superposition of tiles and no gaps between them. For a long time, probably beginning in the early 17th century with Kepler, then stretching through a gap of inactivity that lasted through the 1970s and another through the 2020s, tilings constituted a subject of almost exclusively mathematical interest. The main problem was to find the smallest possible set C that could tile the plane aperiodically (i.e., with endless pattern diversification as the only possibility). The first serious candidates are due to Penrose, first with six edge-marked tile types that completed Kepler's early attempts [1], then with two tile types [2]. It took another half century for Smith et al. [3, 4] to reveal the first solutions with one single tile type.

One of the two-tile type sets from Ref. [2] has had a lasting impact in the field of crystallography, where it suggested structural ordering outside the classical approach [5], prefiguring the discovery of quasicrystals [6] and influencing the field ever since [7]. Other applications of the Penrose tile sets include, e.g., the study of graph-theoretic properties of the classical dimer model [8]. Moreover, the very notion of “aperiodicity” underlying them has been strongly influential, e.g., in interpreting the results of self-assembled crystal structures from molecular building blocks [9], and demonstrating the use of “algorithmic” self-assembly of DNA strands into cellular automata.¹ Self-assembled systems are now part of

cutting-edge research in fields like materials science [12] and DNA-based computing [13–16].

Issues of periodicity, however, become meaningless when the focus shifts toward tilings of bounded regions of the plane, which is the case with applications like modeling biological tissues [17–19] and their properties [20, 21], and developing bioinspired metamaterials [22]. Given finiteness, the central issue is to count the number of distinct tilings that the tile-type collection C admits. Such counting opens the way to calculating all sorts of useful statistical properties, though one must reckon with the fact that only very rarely is it obtainable from a closed-form expression. In this work, we consider K -cell one-dimensional tiles, or K -mers, exclusively.

Given a rectangular region of $m \times n$ square (1×1) cells, already for arbitrary $m, n \geq 2$ it seems that a closed-form expression for how many distinct tilings C admits is known only if C comprises dimers exclusively [23, 24]. Beyond this, fixing $m = 2$ and leaving n unconstrained while monomers and dimers are the allowed tile types seems to be as far as one can go with recurrence relations and generating functions (see, e.g., Ref. [25]). These limitations notwithstanding, two powerful approaches for asymptotic analysis have been used successfully on rectangular regions: the transfer-matrix method (assuming the region of interest either to be a lengthy strip [26] for tiling with Penrose tiles, or to have some form of periodic boundaries on one of the dimensions—see Refs. [27] for trimers, [28] for K -mers with fixed K , and references therein); and the Wang-Landau method [29, 30] for state (tiling) density estimation (see Ref. [31] for assorted K -mers with $K = 1, 2, 4$).

* Corresponding author: srsouza@if.ufrj.br

¹ Specifically, one based on Wolfram's elementary rule 90, the XOR

rule [10]; see Ref. [11] and references therein.

Here we consider the tiling of the $m \times n$ region when C contains every K -mer for $1 \leq K \leq \max\{m, n\}$. We constrain the use of any one tile by the following maximality condition. Placing a tile horizontally requires it to be abutted at each end by a vertically positioned tile; placing the tile vertically requires the abutting tiles to be positioned horizontally. We also assume periodic boundary conditions on both dimensions, which immediately precludes the use of an m -mer vertically or an n -mer horizontally while at the same time abiding by maximality. Thus, given periodic boundaries, we revise the set C to contain every K -mer for $1 \leq K \leq \max\{m, n\} - 1$, along with two circular bands, one with m cells and one with n cells. Taken together, the maximality requirement and the assumption of periodic boundaries have the potential of simplifying the state space, and consequently allowing a cleaner application of the transfer-matrix method, which seems like a natural choice in this case.

Given an assignment of Ising-like states to the $m \times n$ cells (state -1 or $+1$), each resulting K -mer, with its own particular value of K , is a sequence of K cells with like states, arranged horizontally (all cells in state -1) or vertically (all cells in state $+1$), provided tile maximality is respected. Likewise, cells in each resulting m -cell band are all in state $+1$ and cells in each resulting n -cell band are all in state -1 . In all our analyses, an energy function is used that adds up contributions from every pair of juxtaposed cells. Each of the possible contribution values depends on four model parameters, viz., f_L , f_U , g_L , and g_U , taking into account the two cells' states (f_L and g_L for like states, f_U and g_U for unlike states) and juxtaposition directions (f_L and f_U for horizontal, g_L and g_U for vertical). This allows for a rich variety of systems to be represented and likewise for several observables to be studied.

We continue by detailing our theoretical framework in Section II, presenting our results in Section III, and concluding in Section IV.

II. THEORETICAL FRAMEWORK

The tilings consist of two qualitatively different tiles: horizontal and vertical, as illustrated in Fig. 1. The former are associated with cell spins $s = -1$ whereas the latter with $s = +1$, in analogy with the Ising model. The surface on which the tiles are arranged consists of m rows and n columns. Since the transfer matrix method is adopted throughout this work, periodic boundary conditions are imposed along the horizontal axis. For simplicity, the vertical axis is also wrapped around, so the tiling is performed on a toroidal geometry.

A. Energy

The interaction between the different constituents of the system is restricted to nearest neighbors, i.e., a cell

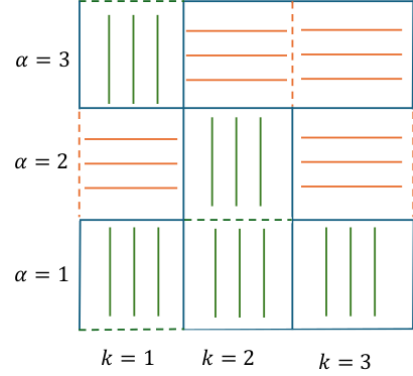


FIG. 1. Example of a tiling for $m = n = 3$. The coordinates are chosen so that the origin is located at the bottom left corner. Cell state -1 is represented by horizontal stripes, cell state $+1$ by vertical stripes. The row and column indices increase from left to right and from bottom to top, respectively. Owing to the periodic boundary conditions, two horizontal and two vertical dimers are present in this configuration. For details, see the text.

located at row α and column k , (α, k) , interacts only with those at $(\alpha \pm 1, k)$ and $(\alpha, k \pm 1)$. For simplicity, there is no self-energy term. By denoting the configuration of a row α as $\mu_\alpha = \{s_1^{(\alpha)}, s_2^{(\alpha)}, \dots, s_n^{(\alpha)}\}$, the energy associated with two adjacent rows is written as

$$E(\mu_\alpha, \mu_{\alpha+1}) = \frac{1}{2} \sum_{k=1}^n \left\{ h_{k,k+1}^{(\alpha)} + h_{k,k+1}^{(\alpha+1)} \right\} + \sum_{k=1}^n v_{\alpha,\alpha+1}^{(k)}, \quad (1)$$

where

$$\begin{aligned} h_{k,k+1}^{(\alpha)} = & \frac{f_L}{4} (1 + s_{\alpha,k}) (1 + s_{\alpha,k+1}) \\ & + \frac{f_U}{4} [(1 + s_{\alpha,k}) (1 - s_{\alpha,k+1}) \\ & + (1 - s_{\alpha,k}) (1 + s_{\alpha,k+1})] \end{aligned} \quad (2)$$

and

$$\begin{aligned} v_{\alpha,\alpha+1}^{(k)} = & \frac{g_L}{4} (1 - s_{\alpha,k}) (1 - s_{\alpha+1,k}) \\ & + \frac{g_U}{4} [(1 + s_{\alpha,k}) (1 - s_{\alpha+1,k}) \\ & + (1 - s_{\alpha,k}) (1 + s_{\alpha+1,k})]. \end{aligned} \quad (3)$$

Above, f_L , f_U , g_L , and g_U are model parameters. They are intended to mimic the interaction between two adjacent pairs and the corresponding contribution to the system energy. The subscripts L and U refer to interactions between two like and unlike cells, respectively. The energy term $E(\mu_\alpha)$ corresponding to pairs lying along the row α is not explicitly included, in order to avoid double counting. In this way, the total energy of the system is obtained by summing the terms given by Eq. (1) over all adjacent row pairs.

One should note that the cells $(1, 2)$ and $(2, 2)$ in Fig. 1 form a maximal tile and give a null contribution to the

total energy. In contrast, the pair (1, 1)-(1, 2) contributes f_L to it. In the same vein, the pair (3, 2)-(3, 3) also forms a maximal tile, giving no contribution to Eq. (1), whereas the pair (2, 3)-(3, 3) adds g_L to it. Furthermore, cell pairs made up of different tiles along the vertical direction, such as (1, 3)-(2, 3), add g_U to the total energy, whereas those along the horizontal direction, such as the pair (2, 2)-(3, 2), contribute f_U . Thus, a convenient choice for the parameters enables one to study the properties of isotropic and anisotropic systems. Finally, due to the periodic boundary conditions, pairs (1, 1)-(1, 3) and (2, 1)-(2, 3) form maximal tiles, while the pairs (1, 2)-(3, 2) and (1, 3)-(3, 3) contribute g_U each to the total energy, and (3, 1)-(3, 3) adds f_U to it.

B. Observables

The above formulation allows one to write the element $\langle \mu_\alpha | P | \mu'_\alpha \rangle$ of the transfer matrix P as

$$\langle \mu_\alpha | P | \mu'_\alpha \rangle = e^{-\beta E(\mu_\alpha, \mu'_{\alpha+1})}, \quad (4)$$

where $\beta = 1/T$ and T is the canonical temperature. The Helmholtz free energy may thus be written as

$$F(T) = -mT \log(\lambda_1), \quad (5)$$

where λ_1 symbolizes the largest eigenvalue of the transfer matrix. We take $m = 50$ throughout this work, except where stated otherwise. This value is sufficiently large to allow us to neglect the further terms associated with the smaller eigenvalues of the transfer matrix in the Helmholtz free energy without qualitatively affecting the quantities we are interested in.

Owing to the complexity of the transfer matrix, the eigenvalues cannot be obtained analytically, so we must use discrete values of T within a convenient range. This range depends on the parameters used in the calculation of the system's energy. The range $0.1 \leq T \leq 10.0$ with steps of $\delta T = 0.1$ is sufficient to highlight the relevant features of the underlying physics in most of the points addressed in this work.

III. RESULTS

We begin by examining the heat capacity of the system, given by

$$C_V = -T \left(\frac{\partial^2 F}{\partial T^2} \right)_V, \quad (6)$$

for $V = mn$, which is easily calculated with the help of Eq. (5) and the standard numerical formulas for derivatives [32]. Its behavior as a function of T is displayed in Fig. 2, for different system sizes and the parameter

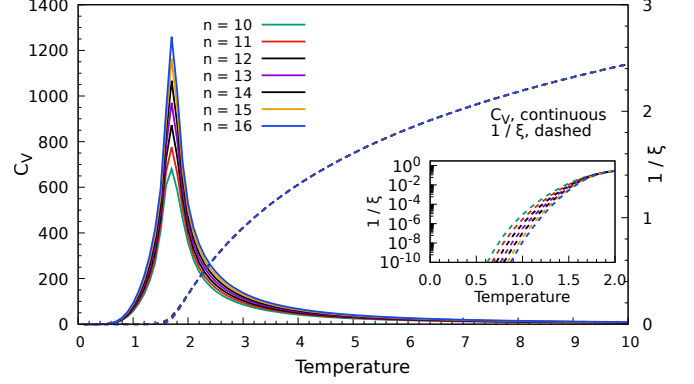


FIG. 2. Left axis: Heat capacity for different system sizes, obtained with $f_L = 1$, $f_U = 2$, $g_L = 1$, and $g_U = 2$. Right axis: The inverse of the correlation length for the same system sizes and parameters. Continuous lines represent the heat capacity while dashed lines depict the inverse of the correlation length. For details, see the text.

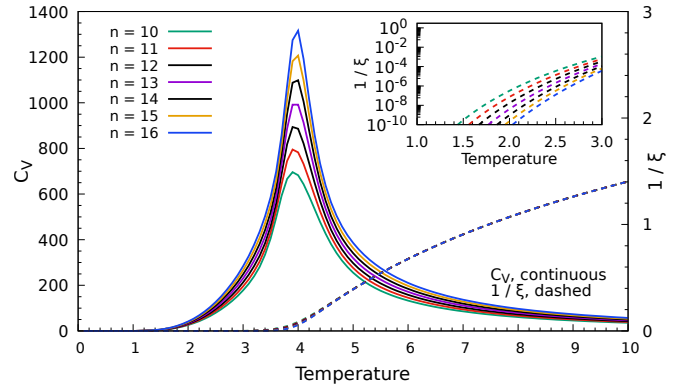


FIG. 3. Same as Fig. 2, now for $f_L = 1$, $f_U = 4$, $g_L = 1$, and $g_U = 4$.

set $f_L = g_L = 1$, and $f_U = g_U = 2$. It reveals that C_V is sharply peaked at $T_c \approx 1.7$, and that the height of the peak increases nearly linearly with system size. These features suggest the occurrence of a second-order phase transition. To examine this aspect more closely, Fig. 2 also displays the inverse correlation length, ξ^{-1} . This quantity is calculated from the eigenvalues of the transfer matrix as in

$$\xi = 1 / \log(\lambda_1 / \lambda_2), \quad (7)$$

where λ_2 corresponds to the second largest eigenvalue. The results show that ξ^{-1} is large at high temperatures, meaning the system is in disordered states. However, the correlation length, ξ , rapidly increases as the temperature approaches T_c , which is a typical signature of a phase transition and indicates that the system is reaching ordered configurations. Nevertheless, the linear scale makes it difficult to assert whether the divergence will also take place at $T = T_c$. The inset shown in the figure seems to indicate that this might occur, as the divergence

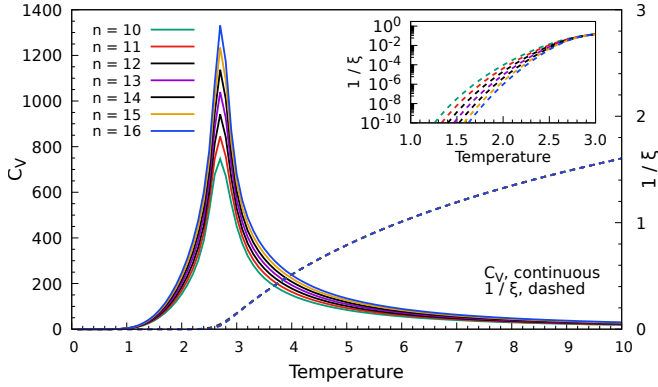


FIG. 4. Same as Fig. 2, now for $f_L = 1$, $f_U = 2$, $g_L = 1$, and $g_U = 4$.

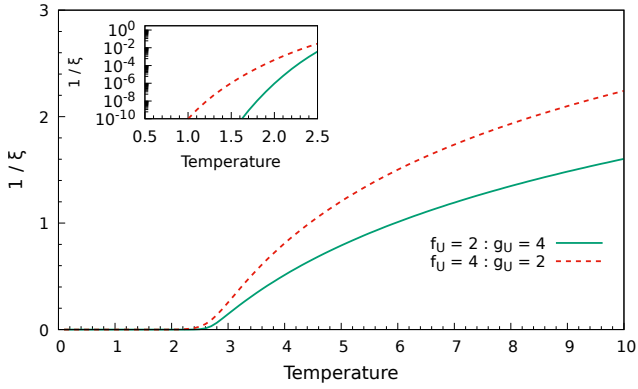


FIG. 5. Inverse of the correlation length as a function of temperature for $n = m = 16$ and different values of f_U and g_U (see legends). In both cases, $f_L = g_L = 1$. For details, see the text.

moves toward T_c with increasing system size. The differences are likely due to finite system-size effects. We come back to this point below.

To examine the sensitivity of our findings to model parameters, we increase the cost of having a tiling with unlike neighbors by setting $f_U = g_U = 4$, while keeping $f_L = g_L = 1$. The corresponding results, shown in Fig. 3, reveal that the same qualitative features persist. The main differences are a shift in the critical temperature to $T_c \approx 4.0$ and broader peaks. We find the same behavior for the correlation length as observed previously. Therefore, these results also suggest that this system undergoes a phase transition as it cools down to T_c , the latter depending on the model parameters.

Among the different qualitative tilings, it is possible to imagine a surface where vertical tiles are more lenient toward horizontal neighbor tiles and vice versa. The results for the parameter set $f_L = 1$, $f_U = 2$, $g_L = 1$, and $g_U = 4$ are shown in Fig. 4. Once more, the same qualitative features are observed, which gives support to the robustness of our findings. We do not show the symmetric case, $f_L = 1$, $f_U = 4$, $g_L = 1$, and $g_U = 2$, as it

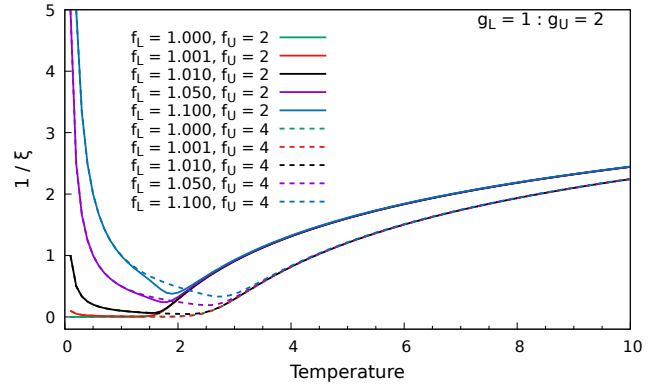


FIG. 6. Inverse of the correlation length as a function of temperature for $n = 10$ and different parameter values. For details, see the text.

would lead to the same qualitative conclusions regarding the global thermodynamic observables. This is due to the fact that the total energy depends on the total number of bonds, which is given by the sum over all vertical and horizontal interactions. Owing to the periodic boundary conditions, the number of horizontal and vertical bonds is identical if the same number of rows and columns are employed. By making $f_U \leftrightarrow g_U$, it is only the costs between bonds that are exchanged. Since the order in the sum of the terms in the total energy is not relevant, the partition function is not affected. We have checked that the quantitative differences are due to the doughnut geometry of the surface and that strictly the same global thermodynamic quantities are obtained, if we use the same number of rows and columns.

On the other hand, the correlation length has directional properties as it propagates the correlations from one row to another and the Hamiltonian of our model is not symmetric under a 90° rotation. Therefore, one should expect differences in ξ by reversing $f_U \leftrightarrow g_U$. This is indeed observed in Fig. 5, where we show the results for $n = m = 16$, so that the differences must be attributed to the symmetry breaking inherent to the Hamiltonian.

A closer inspection of the correlation length provides further information about the characteristics of our system. Figure 6 shows ξ^{-1} as a function of the temperature for slightly different values of $f_L \geq 1$, while the other parameters are kept fixed. We first note that the behavior at high temperature is dominated by f_U . More precisely, a higher cost for having unlike neighbors leads to a more ordered system, as mixed tiles would add a significant number of terms proportional to f_U to the total energy. At lower temperatures, the curves are grouped according to the cost of having similar neighbors. This is consistent with a phase transition where ordered configurations tend to dominate. Nevertheless, the system's tendency toward an ordered phase vanishes as $T \rightarrow 0$, with the exception of the case where $f_L = 1$.

This behavior can be understood by examining the

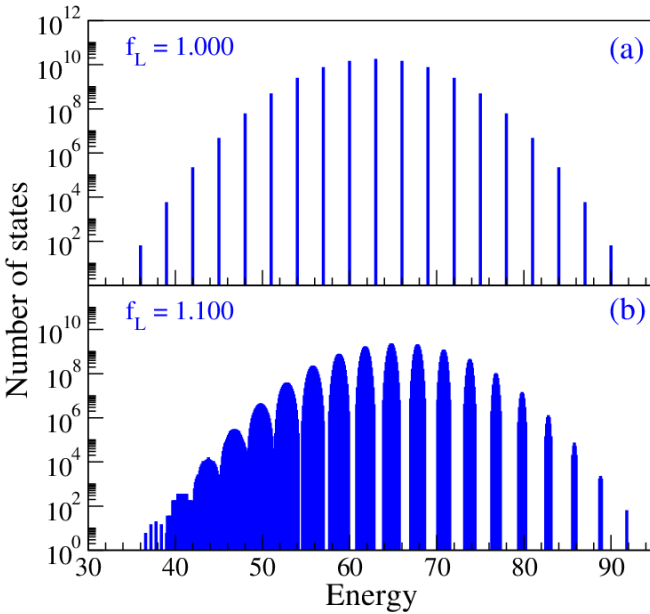


FIG. 7. Number of states as a function of energy for $n = m = 6$, $g_L = 1.000$, and $f_U = g_U = 2.000$. Panel (a): $f_L = 1.000$; Panel (b): $f_L = 1.100$. For details, see the text.

number of states of the system at low energies. Panel (a) of Fig. 7 shows the results for $f_L = 1$, which corresponds to the case where $\xi^{-1} \rightarrow 0$ as $T \rightarrow 0$. Here we see that the ground state is degenerated and the energy landscape consists of narrow and well-spaced peaks. This allows the system to enter an ordered phase with residual entropy at low temperatures, since the Boltzmann factor will not give important contributions above the ground state due to the large barrier. By contrast, for $f_L = 1.1$, the system behaves like a spin glass. Indeed, panel (b) of this figure shows, in turn, a very complex energy landscape, exhibiting many levels close to each other, almost continuously over a large energy range. The existence of many states near the ground state, separated by very low barriers, causes the system to become trapped in different states as the temperature is lowered, preventing it from reaching the true ground state. This leads to a disordered phase, which is a typical characteristic of spin glasses.

The above discussion is based on $n = m = 6$. We did not extend these calculations to larger systems due to the huge increase in the number of states with system size. Reliable estimates, such as those provided by the Wang-Landau method, are beyond the scope of the present work and we simply generated the states one by one. The use of larger systems would lead to lower energy barriers, which would corroborate our conclusions. The sensitivity of the energy landscape to f_L may be inferred from Fig. 8, which shows the entropy

$$S = - \left(\frac{\partial F}{\partial T} \right)_V \quad (8)$$

as a function of temperature for $n = 16$ and different

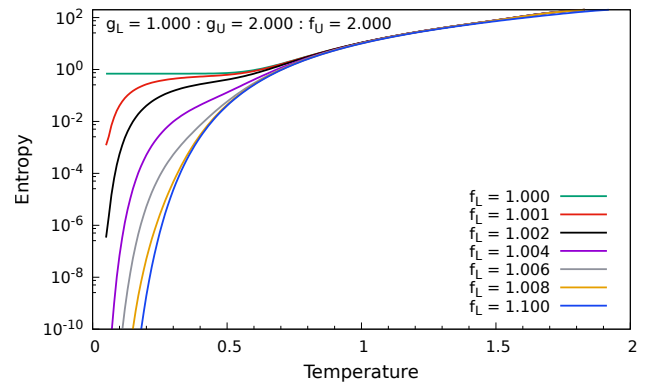


FIG. 8. Entropy as a function of temperature for $n = 16$. For details, see the text.

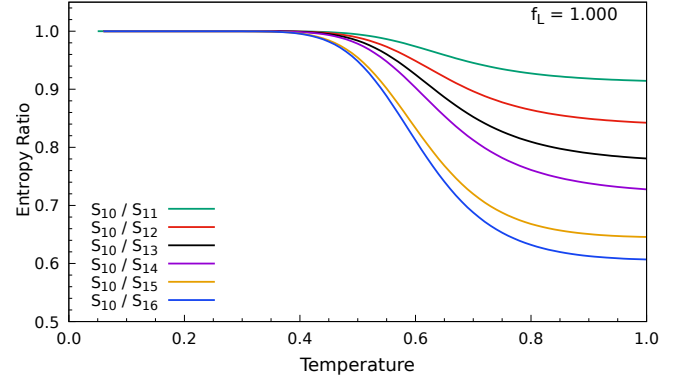


FIG. 9. Ratio of the entropy at $n = 10$ to the entropy of different system sizes versus temperature. The parameters are set to $f_L = g_L = 1.000$, $f_U = g_U = 2.000$. For details, see the text.

values of f_L , while keeping the other parameters fixed. Owing to numerical limitations, the calculations do not include $T = 0$ and have been carried out down to the smallest possible T values. It is clear that the ground state is degenerate for $f_L = 1$ and that the departures from the flat behavior of S appear even for very small deviations from $f_L = 1$. The qualitative conclusions obtained with the calculations employing $n = 6$ still hold in the present case.

The residual entropy seen in Fig. 8 for $f_L = 1$ is also observed in larger systems. This is illustrated in Fig. 9, in which we plot the ratio of the entropy for $n = 10$ and larger sizes. The results show that the ratios are equal to 1 up to $T \approx 0.4$, corresponding to the point at which the entropy deviates from the constant value in Fig. 8 for $f_L = 1$. We therefore conclude that $f_L = 1$ acts as a phase boundary separating two qualitatively different behaviors: An ordered phase with residual entropy for $f_L = 1$ and a disordered spin glass-like phase for $f_L > 1$.

Finally, Figs. 2–4 suggest that the critical temperature extracted from the ξ^{-1} vs. T plot would converge to the values obtained in the plots of C_V vs. T . We have ex-

amined this point by plotting the temperatures at which $\xi^{-1} = 10^{-8}$ for different system sizes and parameter sets. The results are shown in Fig. 10. The horizontal lines in this figure correspond to the T_c values obtained from the peaks of C_V . The trends suggest that the curves would intercept the T_c lines, but it is difficult to draw precise conclusions regarding this aspect through the transfer-matrix method due to computational constraints. Monte Carlo simulations may be helpful in this context but it is beyond the scope of the present study.

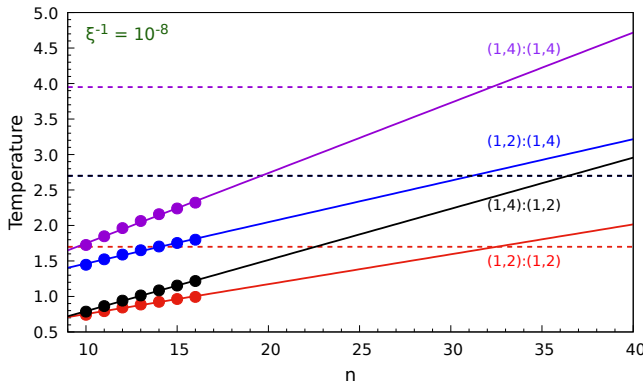


FIG. 10. Temperature at which $\xi^{-1} = 10^{-8}$ for different system sizes and parameter sets $(f_L, f_U) : (g_L, g_U)$. The horizontal lines correspond to the critical temperatures deduced from the heat capacity. One should note that T_c is the same for $(1, 2) : (1, 4)$ and $(1, 4) : (1, 2)$, and for this reason, the corresponding horizontal lines coincide. For details, see the text.

IV. CONCLUDING REMARKS

In this work, we have introduced a new class C of admissible tile types, each type being a K -mer with $1 \leq K \leq \max\{m, n\} - 1$, an m -cell circular band, or an n -cell circular band. However, C has turned out to

be essentially perfunctory, since what is really at stake is whether all the different values of K intended for concomitant use can give rise to at least one tiling for which the property we have called tile maximality holds. While requiring tile maximality introduces a substantial theoretical innovation into the study of tilings, pragmatically a central issue related to requiring maximality has been to demonstrate the use of the transfer-matrix method to analyze tilings admitting the concomitant use of more than one value of K . As one can see from our comments in Section I, thus far this had not been achieved.

As we have demonstrated in Sections II and III, the availability of the system's transfer matrix, especially its two largest eigenvalues, has enabled the identification of a parameter-dependent critical temperature, at which heat capacity peaks. It has also enabled the use of two important analytical tools, viz., the system's correlation length and entropy. For the energy function we adopted, putting all these elements to use has resulted in the identification of a particular parameterization for which a phase boundary occurs, separating an ordered phase from a disordered one.

Moving on to larger systems and possibly different energy functions will likely require the use of Monte Carlo methods and, with them, the availability of more powerful computational resources. We believe that our previous experience with the Wang-Landau method in closely related problems [31] is bound to make a difference.

ACKNOWLEDGMENTS

This work was supported in part by the Brazilian agencies Conselho Nacional de Desenvolvimento Científico e Tecnológico (CNPq) and Fundação de Amparo à Pesquisa do Estado do Rio de Janeiro (FAPERJ), and the Uruguayan agencies Programa de Desarrollo de las Ciencias Básicas (PEDECIBA) and Agencia Nacional de Investigación e Innovación (ANII). This work has been conducted as part of the project INCT-FNA, Proc. No. 464898/2014-5.

[1] R. Penrose, *Bull. Inst. Math. Appl.* **10**, 266 (1974).
[2] R. Penrose, *Eureka* **39**, 16 (1978).
[3] D. Smith, J. S. Myers, C. S. Kaplan, and C. Goodman-Strauss, *Comb. Theory* **4(1)**, #6 (2024).
[4] D. Smith, J. S. Myers, C. S. Kaplan, and C. Goodman-Strauss, *Comb. Theory* **4(2)**, #13 (2024).
[5] A. L. Mackay, *Physica A* **114**, 609 (1982).
[6] D. Shechtman, I. Blech, D. Gratias, and J. W. Cahn, *Phys. Rev. Lett.* **53**, 1951 (1984).
[7] X. Zeng, B. Glettner, U. Baumeister, B. Chen, G. Ungar, F. Liu, and C. Tschierske, *Nat. Chem.* **15**, 625 (2023).
[8] F. Flicker, S. H. Simon, and S. A. Parameswaran, *Phys. Rev. X* **10**, 011005 (2020).
[9] H. Pan and J. Dshemuchadse, *ACS Nano* **17**, 7157 (2023).
[10] S. Wolfram, *Rev. Mod. Phys.* **55**, 601 (1983).
[11] P. W. K. Rothemund, N. Papadakis, and E. Winfree, *PLoS Biol.* **2**, e424 (2004).
[12] N. Kumar, Y.-S. Lan, C.-J. Chen, Y.-H. Lin, S.-T. Huang, H.-T. Jeng, and P.-J. Hsu, *Phys. Rev. Mater.* **6**, 066001 (2022).
[13] D. Woods, D. Doty, C. Myhrvold, J. Hui, F. Zhou, P. Yin, and E. Winfree, *Nature* **567**, 366 (2019).
[14] S. Dey, C. Fan, K. V. Gothelf, J. Li, C. Lin, L. Liu, N. Liu, M. A. D. Nijenhuis, B. Saccà, F. C. Simmel, H. Yan, and P. Zhan, *Nat. Rev. Methods Primers* **1**, 13 (2021).
[15] J. Xu, C. Chen, and X. Shi, *ACS Synth. Biol.* **11**, 2456 (2022).
[16] M. Kim, C. Lee, K. Jeon, J. Y. Lee, Y.-J. Kim, J. G. Lee, H. Kim, M. Cho, and D.-N. Kim, *Nature* **619**, 78 (2023).

- [17] R. Farhadifar, J.-C. Röper, B. Aigouy, S. Eaton, and F. Jülicher, *Curr. Biol.* **17**, 2095 (2007).
- [18] S. Alt, P. Ganguly, and G. Salbreux, *Phil. Trans. R. Soc. B* **372**, 20150520 (2017).
- [19] D. L. Barton, S. Henkes, C. J. Weijer, and R. Sknepnek, *PLoS Comput. Biol.* **13**, e1005569 (2017).
- [20] K. E. Cavanaugh, M. F. Staddon, E. Munro, S. Banerjee, and M. L. Gardel, *Dev. Cell* **52**, 152 (2020).
- [21] J.-A. Park, J. H. Kim, D. Bi, J. A. Mitchel, N. T. Qazvini, K. Tantisira, C. Y. Park, M. McGill, S.-H. Kim, B. Gweon, J. Notbohm, R. Steward Jr., S. Burger, S. H. Randell, A. T. Kho, D. T. Tambe, C. Hardin, S. A. Shore, E. Israel, D. A. Weitz, D. J. Tschumperlin, E. P. Henske, S. T. Weiss, M. L. Manning, J. P. Butler, J. M. Drazen, and J. J. Fredberg, *Nat. Mater.* **14**, 1040 (2015).
- [22] A. Parker, *Phys. Today* **74**, 30 (2021).
- [23] P. W. Kasteleyn, *Physica* **27**, 1209 (1961).
- [24] H. N. V. Temperley and M. E. Fisher, *Philos. Mag.* **6**, 1061 (1961).
- [25] M. Katz and C. Stenson, *J. Integer Seq.* **12**, 09.2.2 (2009).
- [26] F. V. Babalievski, *Physica A* **182**, 325 (1992).
- [27] A. Ghosh and D. Dhar, *Phys. Rev. E* **75**, 011115 (2007).
- [28] L. R. Rodrigues, J. F. Stilck, and W. G. Dantas, *Phys. Rev. E* **107**, 014115 (2023).
- [29] F. Wang and D. P. Landau, *Phys. Rev. E* **64**, 056101 (2001).
- [30] F. Wang and D. P. Landau, *Phys. Rev. Lett.* **86**, 2050 (2001).
- [31] E. J. Aguilar, V. C. Barbosa, R. Donangelo, and S. R. Souza, *Int. J. Mod. Phys. C* **36**, 2450188 (2025).
- [32] M. Abramowitz and I. Stegun, *Handbook of Mathematical Functions* (Dover, NY, 1972).